

Final report for MSc Project

Automated torso soft tissue segmentation for spine modelling in CT scan

Huijing Zhou

Supervisor: Spyros Masouros

Submitted in partial fulfilment of the requirements for the award of MSc in Biomedical Engineering from Imperial College London

Abstract

Torso soft tissue masses and centroids are key parameters in computational spine modelling. These can be extracted from CT scan images.

Building on a previous study on the automated vertebral body height measurement only of the sagittal and coronal planes, this study aims to develop an automated torso soft tissue segmentation algorithm to calculate the areas and centroids of the transverse plane using image segmentation techniques, in order to calculate the masses and the vertebral geometric centroids.

Three upper body CT scan databases were used to evaluate the algorithm. This algorithm was successful in segmenting the soft tissue region as well as removing the CT scanner bed (using 2 methods) and arms (using 2 methods), with an average Dice coefficient of 98.04% and computation time from 5.01s to 28.05s per slice. The CT scanner bed removal method 2 was 4 times on average faster than method 1, while arm removal method 2 was 1% on average more accurate than method 1.

The masses and centroids were calculated, and expressed as the sectional mass percentage, increasing from C1(0.36%) to L5(2.75%). The overall torso mass percentage was 34.82% on average, which provided new reference data on the sectional torso masses.

Acknowledgements

This study has been supported by the Centre for Blast Injury Studies at Imperial College London. The author thanks Lucas Low and Dr.Masouros for their advice, and the University of Virginia for providing the CT scan databases.

1. Introduction

Computational biomechanical modelling is a common approach to studying the spine biomechanics in the field of blast injury[1], [2], automotive injury[3], and lower back pain[4], as those physiological and pathological processes of the spine are closely linked to biomechanical process[5]. By calculating and analysing its coronal deviation, axial rotation and length discrepancies, the movement and damage of the spine can be assessed[6], which can provide the basis for the establishment of clinical diagnostic criteria for some spinal-related diseases such as scoliosis, kyphosis and lordosis[7], in order to guide the surgeons to plan better for the patient's surgery and post-operative recovery[8].

Torso soft tissue masses and centroids are key parameters used in finite element modelling[9], [10] and multi-body modelling[11], [12]. These can be extracted by segmenting torso soft tissue from medical images. Currently, researchers finished the segmenting process mostly manually. Keenan et al. used the “Segmented Line” tool in ImageJ to draw the contours of each target region of transverse slices, completing the calculation of their area and centroids[13]. However, the manual approach is proved to be time-consuming and is prone to an error caused by user fatigue or disagreement between observers[14].

Therefore, researchers have developed multiple automated segmentation algorithms for soft tissue detection[15]–[20]. Popuri used the finite element method deformable model to segment the fat tissue, which could be transformed into torso contours, with a Jaccard coefficient exceeding 90% [15]. For detecting lungs, Than et al. applied Otsu gray level thresholding and morphological filtering combined with Radon transform, with the success rate of 79.0% for the right lung and 92.6% for the left lung[16]. Nithila et al. used selective binary and Gaussian filtering with a new signed pressure force function (SBGF-new SPF)[17], while Dai et al. finished the segmentation using an improved graph cuts algorithm combined with Gaussian Mixture Model (GMM) for lungs detection, with a Dice coefficient (DC) of 98.74% and 10 - 15 min computation time[18]. While the segmentation results can vary depending on the chosen algorithms, thresholding and region growing methods are proved to be with high stability, accuracy and speed[19], [20]. For segmentation result evaluation, DC is usually regarded as a gold standard[21]. It reflects the consistency of the size and localisation compared segmented region with the target region and has become popular after being used in VNET, which is a neural network for volumetric medical image segmentation[22]. However, the previous research only focused on specific tissue extraction (fat, lungs, etc.) with high algorithmic complexity and long computation time. Meanwhile, these algorithms do not involve the arm and the CT scanner bed removal, which may not be suitable for spine modelling. Therefore, a fast and suitable automated algorithm for vertebral-parameter calculation is needed.

To calculate the sectional torso masses and vertebral geometric centroids, an automated algorithm to measure the vertebral body heights (VBHs), intervertebral disc heights (IDHs), vertebral body centroids of the sagittal and coronal planes (7.1) has been developed previously at Imperial College London. This study used 4 methods to measure the VBHs after manual masking of vertebral bodies on the sagittal and coronal planes, and the results from method 4 were the most promising, shown in (7.1). However, this study fell short of segmenting the area for the transverse plane. Therefore, the current study aims (i) to develop an automated torso soft tissue segmentation algorithm based on thresholding and region growing techniques in transverse slices of CT scan and (ii) to use its area in combination with previous research to calculate the sectional torso masses and vertebral geometric centroids.

2. Materials and Methods

2.1. Framework

The framework, Figure 1, aimed to segment the torso soft tissue region and calculate sectional torso masses based on image segmentation algorithms. These included 3 core steps: (1) CT scanner bed removal; (2) Soft tissue segmentation – to subtract body cavity region e.g., lung parenchyma from initial torso region; (3) Arm removal – to remove the arms, as the arms are connected to the shoulders but not directly to the torso. The areas and centroids were obtained directly from the final segmentation result and then combined with the vertebral body height study done at Imperial College (7.1 7.2) to calculate the sectional torso masses.

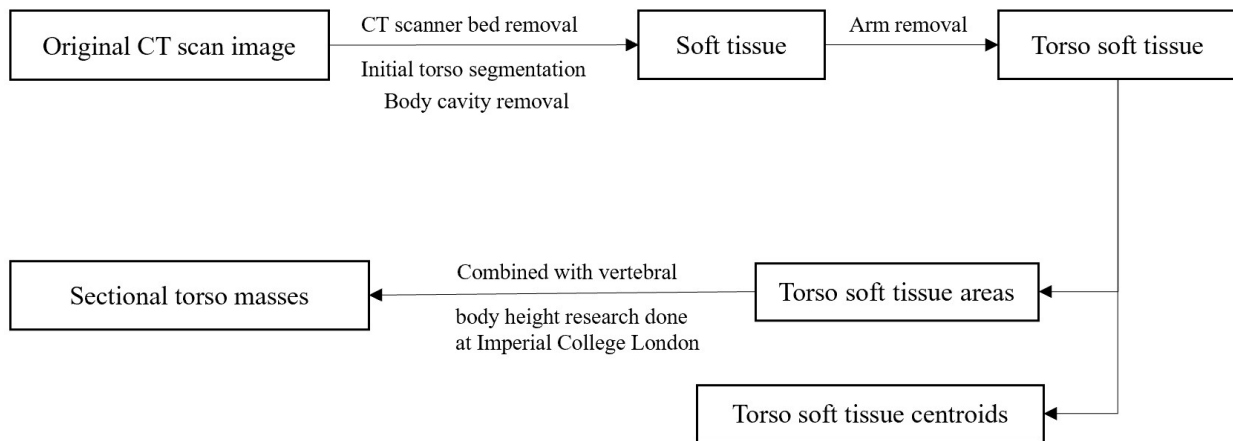


Figure 1: Framework of the current study

2.2. CT Imaging dataset descriptions

Three male cadavers' complete upper body CT scan databases[23], with an average age of 63.33 ± 5.13 yr, an average mass of 90 ± 19.08 kg, and an average height of 178.67 ± 5.13 cm, Table 1, were used to validate the torso soft tissue segmentation algorithm developed in this research. All the data collection procedures were carried out by researchers at the University of Virginia (UVA), and they were approved by the UVA Cadaver Use Committee. Necessary informed consent from three cadavers and/or the support of their families were obtained before data collection, to ensure the legality of using the data.

Three groups of scans were collected by using "GE MEDICAL SYSTEM" under the operation of professional radiologists, with Helical and Dynamic mode respectively. These modes allowed for the better image quality of contrast for substantive organs, which made it easier to perform accurate tissue segmentation. The pixel spacing was 0.976562 mm/pixel and the slice thickness was 0.625 mm for these 3 databases.

Table 1: Specimen characteristics

Specimen	Age (yr)	Mass (kg)	Height (cm)	Gender	Cause of death
606	62	68	173	M	Lung cancer
636	69	100	180	M	Huntington's disease
526	59	102	183	M	Melanoma

2.3. CT bed removal – Method 1 & Method 2

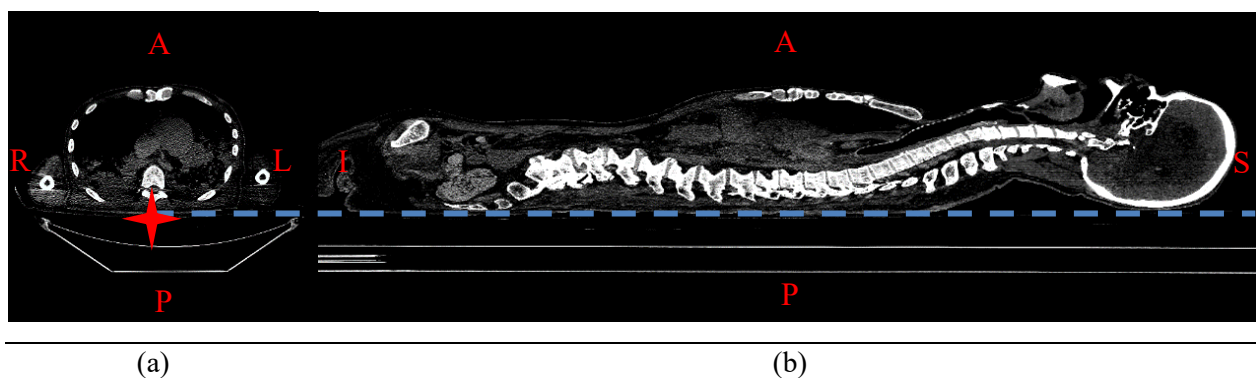
Removing the CT scanner bed is essential for accurate parameter calculation. Thresholding combined with morphological transformations is most used but under the assumption that the projection of the CT scanner bed is not connected to the torso, which is not the usual case when the subject is being scanned[24], [25]. To break this assumption, Zhu et al. proposed an automatic bed removal method based on the edge and line detection in the sagittal plane, which was used in this research, Method 1, with efficient segmentation results but long computation time caused by the sagittal image reconstruction[26]. Meanwhile, to accelerate the process, another method based on the transverse plane was developed in this research, Method 2.

Method 1 – Thresholding combined with sagittal plane edge and line detection algorithm

The transverse projection of the CT scanner bed, Figure 2(a), was not in a regular shape compared with that in the sagittal plane. Its sagittal projection shape, Figure 2(b), was supposed to be straight lines that were perpendicular to the anterior-posterior (AP) axis and parallel to the superior-inferior (SI) axis. Among those straight lines, the top one corresponded to the location of the CT scanner bed top. The AP-coordinate of that was obtained by firstly Sobel operator for edge detection, Figure 2(c), and then Hough transformation for line detection based on those edges. It also represented the location of the CT bed top where the transverse slice met the corresponding sagittal slice. For example, the AP-coordinate of the CT bed top detected on the mid-coronal sagittal plane is the same as that of the midpoint in the left-right (LR) axis of transverse slices. Therefore, one point of CT bed top profile in transverse slices was acquired from one sagittal image at one location. Then, by looping all sagittal slices, the CT bed top profile was obtained, Figure 2(d). As the region below this profile in transverse slices didn't contribute to the torso soft tissue, the CT bed was removed by setting all the grayscale values below to be 0 (background), Figure 2(f).

The key steps and parameter setting of this algorithm were as follows:

- (1) Reformat the dataset to sagittal plane.
- (2) Binarise the sagittal slices with a threshold of -500HU.
- (3) Detect edges by Sobel operator and only retain the AP gradient result, as the lines to be detected only contributed to the AP gradient result.
- (4) Detect straight lines by Hough transformation. Hough transformation can be used for straight line and circle detecting. The detected straight lines together with their AP-coordinates were seen as valid when the number of the connected pixels exceeded 400 and the angle was within $0^{\circ} \pm 0.1^{\circ}$.
- (5) Find the smallest AP-coordinate as one point of the CT scanner bed profile in transverse slices.
- (6) Loop through all the sagittal slices to obtain the profile.
- (7) Set all the grayscale values below the profile to be zero.



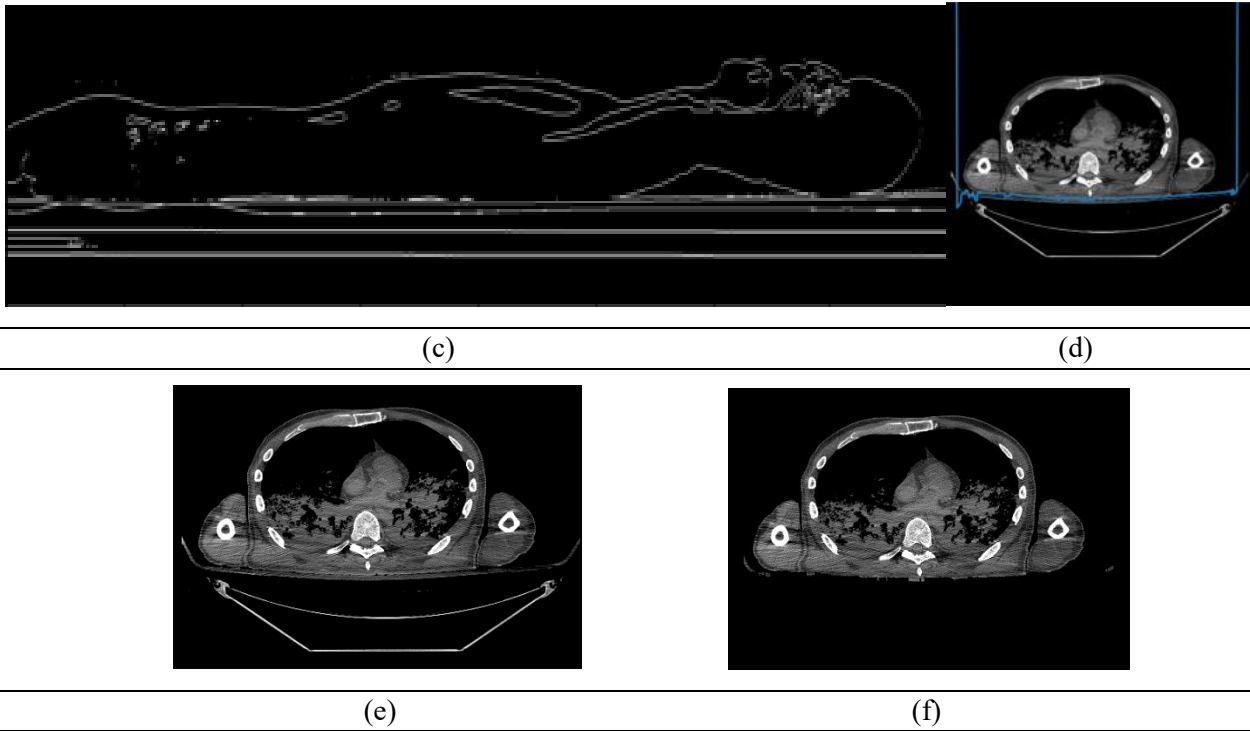
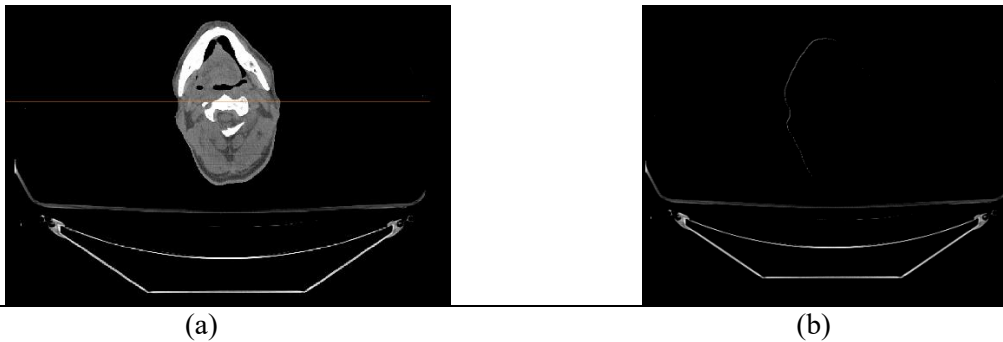


Figure 2: Method 1 to remove the CT scanner bed. (a) The CT bed top in the mid-coronal transverse plane (red cross marker), where A = anterior, P = posterior, L = left, R = right. (b) The CT scanner bed top in the mid-coronal sagittal plane (blue line), where S = superior, I = inferior. (c) The edge detection result was done by the Sobel operator. (d) The CT scanner bed top profile (shown in blue). (e) Original CT image of specimen 606. (f) The image following removal of CT scanner bed.

Method 2 – Fast segmentation based on transverse scanning process static algorithm

The CT scanner bed projection, Figure 3(b), could be more simply extracted from those transverse slices where the CT bed was not connected to the torso (e.g. neck slices), Figure 3(a). It was obtained by first using 2.4 to detect the torso region, and then setting the grayscale values of this region in the original image to be 0 (background). Under the assumption that the CT scanner bed had a uniform transverse projection during one specimen's scanning process, this CT bed projection was the same for all the other transverse slices. Therefore, when processing other slices, their CT scanner bed region could be removed by setting the grayscale value of this CT bed region in target slices to be 0 before other subsequent processing, Figure 3(d).



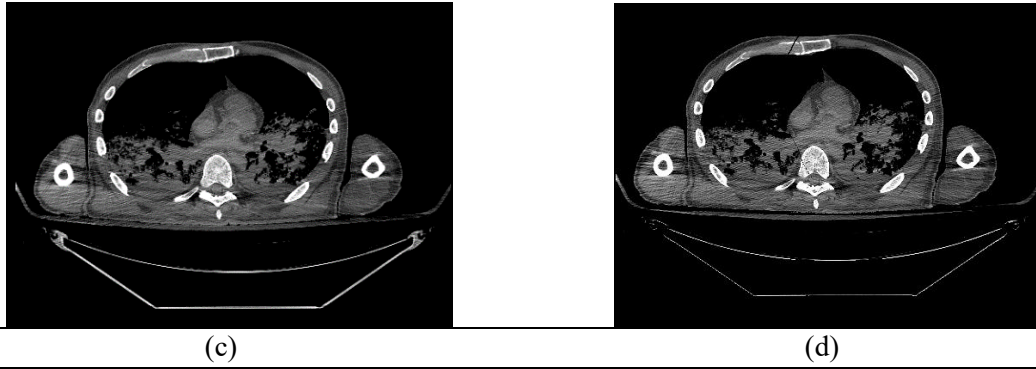


Figure 3: Method 2 to remove the CT scanner bed. (a) Original CT image for CT bed region detection. (b) The CT scanner bed projection. (c) Original CT image. (d) The image following removal of CT scanner bed.

2.4. Soft tissue segmentation – Binarisation and morphological transformation

The soft tissue region of transverse slices, Figure 4(b), was obtained by subtracting the body cavity mask from the initial torso (torso and arms) mask.

Initial torso mask, Figure 4(a), was detected by thresholding in combination with connected-component analysis (CCA). The key steps and parameter setting of this algorithm were as follows:

- (1) Enhance soft tissue region contrast by contrast stretching, with the stretching range from -150 HU to 350 HU.
- (2) Binarise the image, with the threshold set to 0.
- (3) Remove background noise, which was shown as some small spots caused by the CT scanning process, using closing (one of the morphological transformations), with a 2-pixel circular structural unit kernel.
- (4) Detect the largest connected area by CCA, with 8-connected pixels.
- (5) Fill all the holes of the largest connected area to get the initial torso mask.

The body cavity mask was obtained by the following 2 steps:

- (1) The initial body cavity mask was obtained by subtracting the largest connected area from the initial torso mask.
- (2) Remove regions whose areas were less than 15 pixels. These regions should be in soft tissue but were classified in the body cavity because the CT artefacts resulted in a grayscale value below -150 HU in those regions, which needed to be corrected.

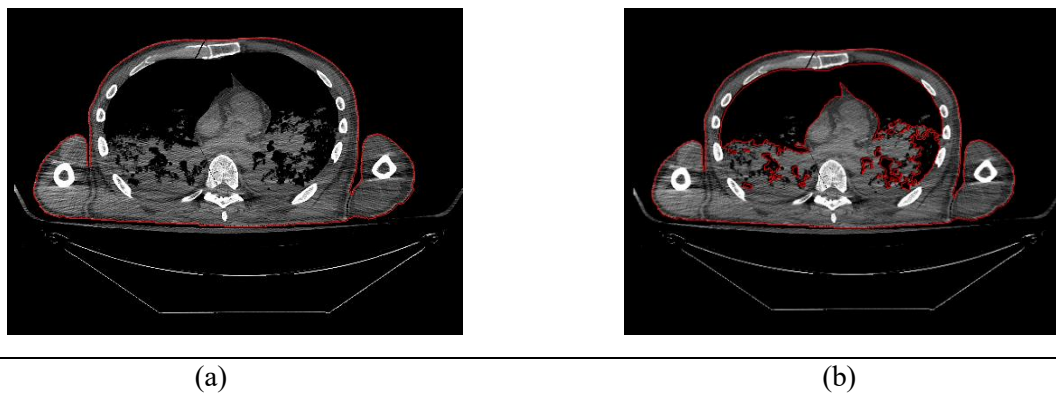


Figure 4: Soft tissue segmentation. (a) Initial torso region (its contour shown in red). (b) Soft tissue region (its contour shown in red).

2.5. Arm removal – Method 1 & Method 2

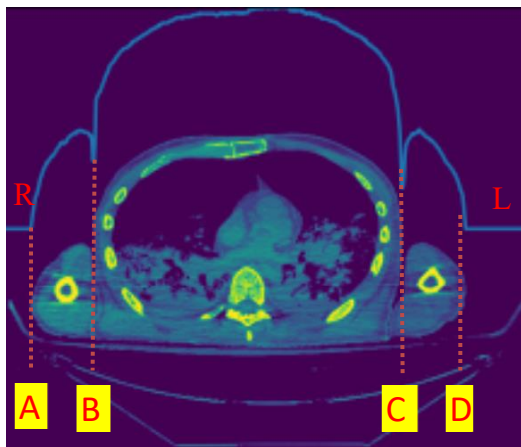
The soft tissue mask obtained from 2.4 would contain the arms if the arm were connected to the torso in transverse slices. Those arm regions needed removing in this step. Gong proposed an automated arm removal method that required sagittal and coronal plane reconstruction, which contributed to the computation time[27]. Therefore, a more simplified method, Method 1, was developed to process directly on the transverse slices based on the same idea that to cut arms directly from the vertical. These two vertical arm-cutting methods assumed that both arms were located on the left and right sides of the torso[27]. Therefore, they could not detect the arm edges and were not efficient for the subjects who placed their forearms on the abdomen (specimen 636 and 526), where the arms were in the diagonal or upper part of the torso in transverse slices. For these specific situations, a region growing based arm removal algorithm, Method 2, was developed here.

Method 1 – Vertical arm-cutting algorithm in transverse slices

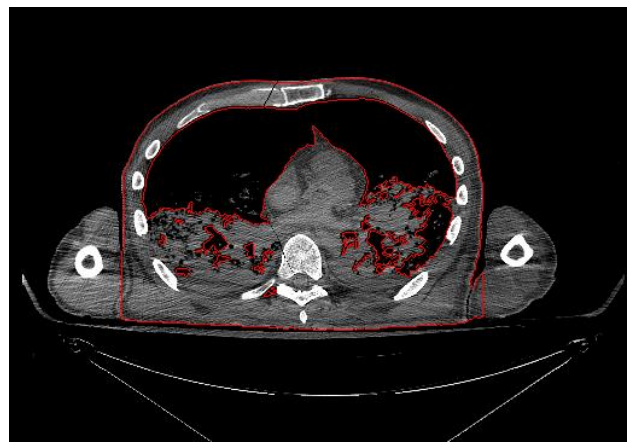
This method assumed that both arms were located on the left and right sides of the torso, which was more common for most upper body databases. From transverse slices, the arm projections, Figure 5(a), ranging from A to B and C to D, existed independently in AP-axis, i.e. the upper and lower regions in the arm projections didn't include the torso region. Therefore, the left and right arms could be removed by cutting vertically from point B and point C, and the region between point B and C was the torso soft tissue required.

In order to detect point B and point C, a profile, Figure 5(a), was obtained by summing up all the column values of the initial torso mask. This profile reflects the horizontal information of the image. Two dips appeared at the junction of the arms and torso, corresponding to points B and C, Figure 5(a). After flipping the profile and adding the profile maximum value to it, the two dips were converted to two peaks that could be detected using peak detection.

After detecting the LR-coordinates of points B and C, the left and right arms could then be removed by setting the pixel value whose LR-coordinates ranged from 0 to point B and point C to the image width to be 0, Figure 5(b).



(a)



(b)

Figure 5: Method 1 to remove the arms. (a) Original CT image and its profile (shown in blue) by column summation, where points A B C and D represent the R-side arm edge, R-side arm and torso junction, L-side arm and torso junction, L-side arm edge respectively. (b) Segmented region (its contour shown in red).

Method 2 – Watershed algorithm for arm removal

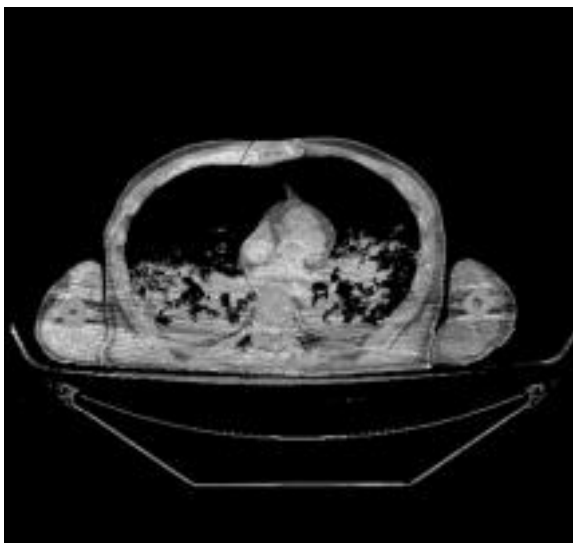
The watershed algorithm is a region growing based image segmentation algorithm that is primarily applied to segmenting overlapping objects. It considers the image as a topography map, where the intensity of the image contributes to the map. High-intensity regions are seen as the peaks, while the low-intensity regions are seen as the valleys, i.e. the local minima. To separate overlapping objects, each valley needs to be filled from the local minima based on the grayscale value gradient until valleys start to merge [28]. Those merged lines are regarded as edges required to separate arms and torso.

The intensity of bones was high in the CT scan so that they could be regarded as edges when segmenting the arms, which led to incomplete arm masks. Therefore, bone contrast needed to be removed with the following steps. Firstly, contrast stretching, ranging from 150 HU to 1000 HU, was applied to segment bone regions in the image. Then the bone mask was obtained by thresholding, with the threshold set to 0. Finally, the bone effect was eliminated by setting the grayscale value of the corresponding region in the bone mask to be 90 HU in the original image, Figure 6(a). This grayscale value was closer to that of the average soft tissue.

Two user-defined markers were used to separate one arm and the torso, which were usually set as two circles with a radius of 40 pixels whose centroids were in the arm and torso respectively and were close to the desired edges. These markers were seen as the local minima of the image and also as the input of the watershed algorithm, so that the two regions representing the arm and torso were obtained. Note that the watershed algorithm should be applied to the original image with bone contrast removal rather than the soft tissue mask, as the mask image didn't show any gradient information. As the arm area was smaller than the torso area, the arm mask was the region with fewer pixels.

For the slices that need to remove the bilateral arms, three markers, Figure 6(b), needed to be defined in the left arm, right arm, and torso respectively. The bilateral arm masks were regarded as the two with the smallest number of pixels.

Finally, the torso soft tissue mask was obtained by setting the grayscale value of the arm mask region in the soft tissue mask to be 0.



(a)



(b)

Figure 6: Method 2 to remove the arms. (a) The CT image after bone contrast removal. (b) Three circular user-defined markers were used as the input for the watershed algorithm.

2.6. Sectional torso parameter calculation

Torso soft tissue area and centroid calculation

Torso soft tissue areas and centroids are needed for calculating sectional torso volumes and masses. The areas A were calculated by Eqn.1), where N represents the number of pixels in the torso soft tissue mask.

$$A = N * Pixel\ spacing^2 \quad 1)$$

The centroid coordinates of the torso soft tissue were calculated by geometric decomposition in the following steps, assuming the tissue density was uniform. Firstly, all the contours of the torso soft tissue mask were detected to extract areas A_i and the moments M_i . Then the centroid coordinates C_{ix} , C_{iy} of each contour were calculated by Eqn. 2), as centroids were the first moment of Area. By geometric decomposition, the overall centroids C_x , C_y could be acquired, Eqn. 3).

$$\begin{aligned} C_{ix} &= \frac{M_{i10}}{M_{i00}} \\ C_{iy} &= \frac{M_{i01}}{M_{i00}} \end{aligned} \quad 2)$$

$$\begin{aligned} C_x &= \frac{\sum C_{ix} A_i}{\sum A_i} \\ C_y &= \frac{\sum C_{iy} A_i}{\sum A_i} \end{aligned} \quad 3)$$

Sectional torso volume and mass calculation

Sectional torso volumes V were given by Eqn. 4), multiplying torso soft tissue area A by the vertebral body thickness T .

$$V = A * T \quad 4)$$

The transverse slices chosen to perform torso soft tissue area A calculation were those that crossed the z-centroids in either coronal or sagittal plane. Relative centroid coordinates c_z are given by 7.1. These were the coordinates after the isometric scaling from the original image, and therefore the true z-centroid coordinate C_z needed to be calculated by Eqn. 5).

$$C_z = L - \left(c_z * \frac{L}{l} \right) \quad 5)$$

where L represents the length of the original image, given by Eqn. 6), and l represents the length of the sagittal and coronal image, shown in 7.2.

$$L = Slice\ thickness * (Slice\ number - 1) \quad 6)$$

where *Slice number* represents the total number of CT scan transverse slices for each database.

Those target transverse slices whose z-coordinates were most close to C_z would be chosen to be applied 2.3 to 2.6 to calculate the torso soft tissue areas and centroids.

The vertebral body thickness T refers to the distance from the upper end of one vertebral body to the upper end of the next vertebral body. Therefore, it includes the vertebral body height VBH and intervertebral disc height IDH , Eqn. 7).

$$T = VBH + IDH \quad 7)$$

After calculating sectional torso volume, the sectional torso mass STM could be calculated by Eqn. 8), based on a single average density $\rho = 1.04 \text{ g/cm}^3$.

$$STM = \rho * V \quad (8)$$

Then the sectional torso mass was expressed as a percentage of the total body mass $STM \text{ Percentage}$, with Eqn. 9), which was used to compared to other papers.

$$STM \text{ Percentage} = \frac{STM}{Mass} * 100\% \quad (9)$$

2.7. Manually segmentation process

The segmented results from the automated algorithm of 3 databases were compared with the manually segmented results done in MIMICS 23.0. This process contained 7 steps as follows:

- (1) Create a new mask called the soft tissue mask and enhance the soft tissue region by setting the thresholds to a soft tissue window from -150 to 350 HU, which is the same as the stretching range in 2.4.
- (2) Locate at those target transverse slices, i.e., the closest transverse slices to C_z calculated in 2.6.
- (3) Use the 'Edit masks' tool to manually remove the CT scanner bed and arm region.
- (4) Use the 'Edit masks' tool to add the bone region. It contributed to the torso soft tissue masses as well but was not included in the newly created soft tissue mask as the bone intensity was higher than 350 HU.
- (5) Use the 'Edit masks' tool to add low-intensity spots inside the soft tissue caused by CT artefacts to obtain the final torso soft tissue mask.
- (6) Set the mask colour to white for the convenience of mask extraction.
- (7) Export all the images in DICOM files, and only set the soft tissue mask visible.

2.8. Evaluation parameter

Dice coefficient

Dice coefficient (DC) is often regarded as a gold standard in image segmentation result evaluation and was used in this study to evaluate the torso soft tissue segmentation accuracy of the automated algorithm, Eqn. 10).

$$DC = \frac{2|A_{segment} \cap M_{segment}|}{|A_{segment}| + |M_{segment}|} * 100\% \quad (10)$$

where $A_{segment}$ represents the torso soft tissue region calculated by automated algorithm from 2.3 to 2.6, and $M_{segment}$ represents the manually masked torso soft tissue region in 2.7.

It essentially measures the overlap between the automated and manually torso soft tissue region, ranging from 0 to 1, and the closer to 1, the better the segmentation result is [21].

Area percentage

Area percentage (AP) was selected here to assess the accuracy of the area calculation, Eqn. 11).

$$AP = \frac{2|A \cap A_{manual}|}{|A| + |A_{manual}|} * 100\% \quad (11)$$

where A represents the torso soft tissue area calculated by Eqn. 1), and A_{manual} represents the manually masked torso soft tissue area that is calculated by Eqn. 12).

$$A_{manual} = N_{manual} * Pixel \text{ spacing}^2 \quad (12)$$

where N_{manual} represents the number of pixels in the manually masked torso soft tissue region.

Computation time

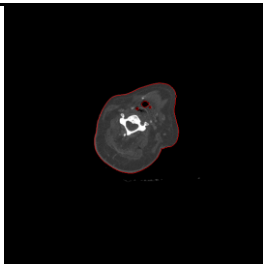
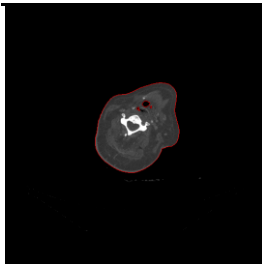
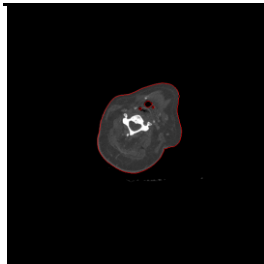
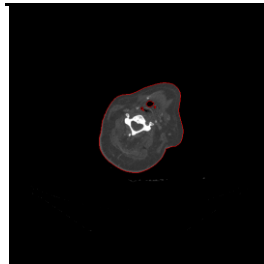
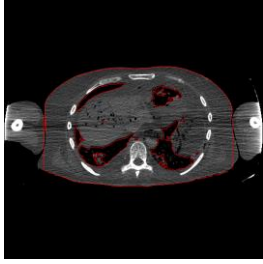
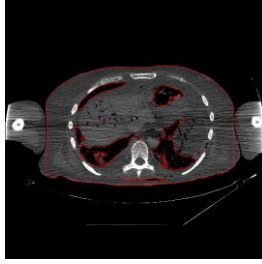
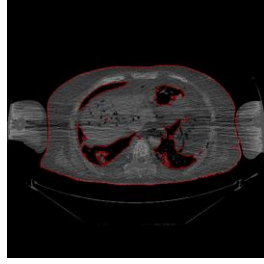
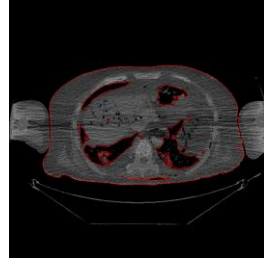
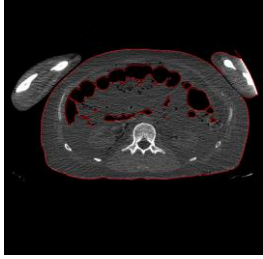
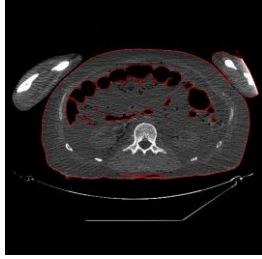
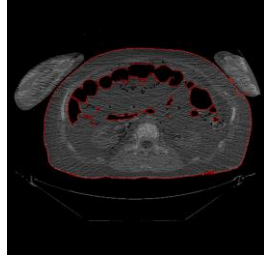
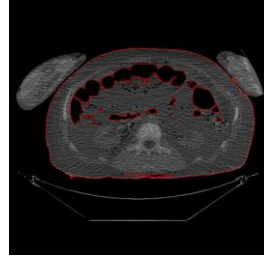
Computation time was used here to evaluate the efficiency of the automated algorithm. This was calculated using the time toolkit in python 3.8 based on an Intel(R) Core(TM) i5-6267U CPU @ 2.9GHz 4CPUs computing environment. Note that the computation time only included the total time the program run, but not the time spent on manually setting up markers and slices.

3. Results

3.1. Torso soft tissue segmentation

After extracting the target transverse slices from 3 databases, 23 slices (from C2 to L5) from database 606, 15 slices (from T3 to L5) from database 636, 24 slices (from C1 to L5) from database 526, where each vertebra corresponds to one target slice, were obtained to complete the torso soft tissue segmentation with the automated segmentation algorithm from 2.3 to 2.5. Segmentation results of levels C3, T8 and L2 in database 526 was shown in Table 2.

Table 2: Torso soft tissue segmentation results of levels C3, T8 and L2 in database 526. Algorithm 1 represents the combination of CT scanner bed removal method 1 and arm removal method 1, Algorithm 2 represents the combination of CT scanner bed removal method 2 and arm removal method 1, Algorithm 3 represents the combination of CT scanner bed removal method 1 and arm removal method 2, Algorithm 4 represents the combination of CT scanner bed removal method 2 and arm removal method 2.

Level	Algorithm 1	Algorithm 2	Algorithm 3	Algorithm 4
C3				
T8				
L2				

The automated segmentation results were evaluated using DCs mentioned in 2.8 compared with the manual segmentation mask created in 2.7. The average DC results for each section of 3 databases are shown in Figure 7, where the DC of C1 only represents the result from specimen 526 and the DCs from C2 to T2 represents the average result from specimen 606 and 526, as the target slice of specimen 636 started from T3.

The DCs of all vertebral levels from C1 to L5 by the 4 combined algorithms were all above 95%, and the average was 98.04(SD 0.82)%. These 4 algorithms showed the least segmenting accuracy in level T7, with an average DC of 96.39(SD 0.82)%, while the best accuracy in C7, with an average DC of 99.05(SD 0.02)%. The 4 combined algorithms performed the best in cervical sections, with an average DC of 98.54

(SD 0.42)%, while performed the worst in thoracic sections, with an average DC of 97.75 (SD 0.78)%. The average DCs of Algorithm 1, 2, 3 and 4 were 97.75(SD 0.95)%, 97.78(SD 0.94)%, 98.32(SD 0.58)%, 98.32(SD 0.56)% respectively. Comparing Algorithm 1 and 2 (both used arm removal method 1) with Algorithm 3 and 4 (both used arm removal method 2), arm removal method 2 (watershed algorithm) showed an advantage at segmenting torso soft tissue. However, there was little difference in DC between CT bed scanner removal method 1 and method 2 when comparing Algorithm 1 and 3 (both used CT scanner bed method 1) with Algorithm 2 and 4 (both used CT scanner bed method 2).

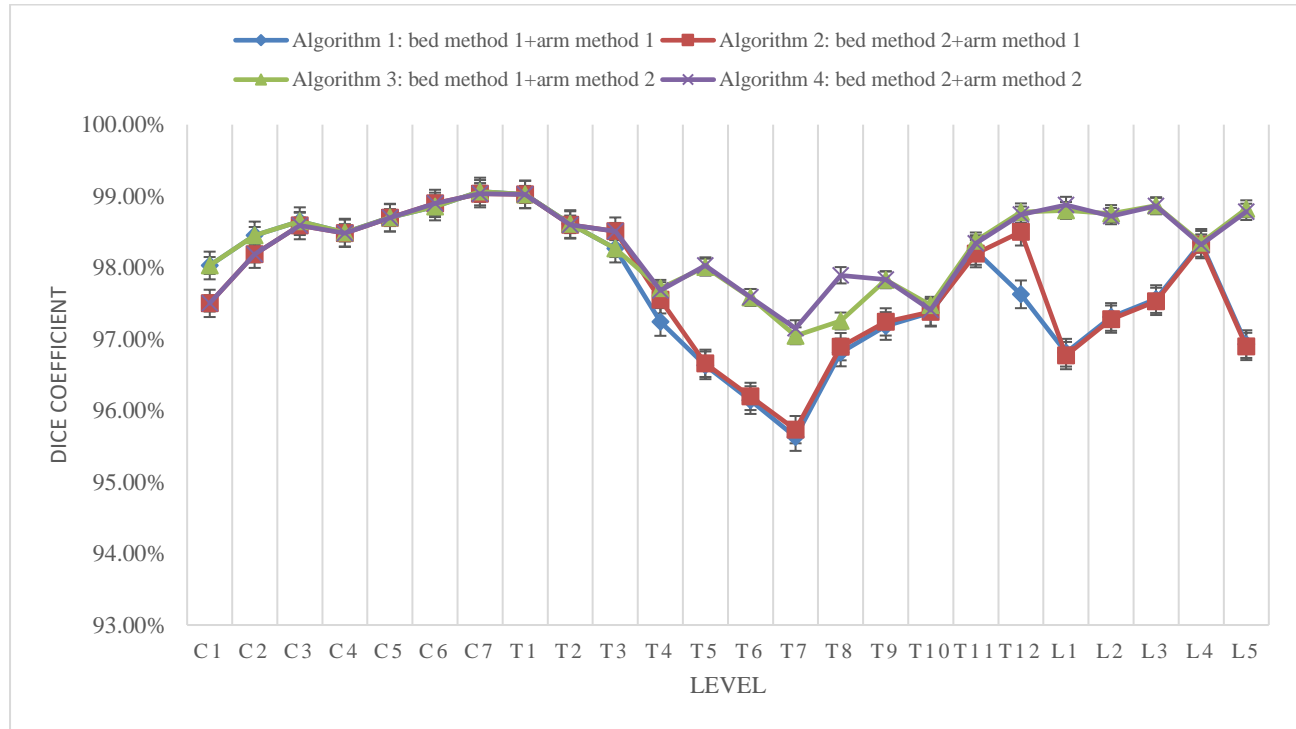


Figure 7: Average dice coefficient of the torso soft tissue segmentation results.

3.2. Computation time

The computation time calculated by 2.8 is shown in Table 3. The average time per slice for Algorithm 1, 2, 3, and 4 was 24.64, 5.01, 28.05, 8.79 s respectively. Comparing Algorithm 1 and 3 (both used bed removal method 1) with Algorithm 2 and 4 (both used bed removal method 2), bed removal method 2 (fast segmentation based on transverse scanning process static algorithm) resulted in an average of 19.45 s faster than method 1. Whereas Algorithm 3 and 4 took an average of 3.60 s more than Algorithm 1 and 2, there was not much difference in arm removal methods in terms of computation time.

Table 3: Computation time for automated algorithms

Specimen	Processed image number	Algorithm 1 (s)	Algorithm 2 (s)	Algorithm 3 (s)	Algorithm 4 (s)
606	23	193.69	37.09	206.03	49.43
636	15	157.34	26.29	188.33	62.89
526	24	137.57	39.41	156.97	58.81

3.3. Torso soft tissue parameters

Table 4 shows the results of the torso soft tissue parameters calculated in 2.6 using Algorithm 4. The average sectional torso soft tissue areas from C1 to L5 showed an upward trend, increasing rapidly from C3 with a local peak around T3 at 63645.93 mm². The average areas of the lumbar were the most stable, with the largest area appearing at T11 at 68779.24 mm².

Influenced by the vertebral body thickness T , the trend of the average sectional torso soft tissue volumes and masses differed from that of the areas. There was an increasing trend from C1 to T3, but a decrease from T3 till T6, then following an increase again till L5, with the maximum volume and mass appearing at L1 at 2350.66 cm³ and 2444.69 g respectively.

The sectional mass percentage of the total body mass, Figure 8, showed an upward trend from C1(0.36%) to L5(2.75%). It started rising quickly from C3 till T5 and appeared a local minimal at T7(1.49%). The maximum mass percentage occurred at L5. Compared with previous studies by Keenan et al. (20 females, mean age 15 years)[13], Pearsall et al. (2 females and 2 males, mean age 61 years)[29] and Duval-Beaupère and Robain (10 males, mean age 27.5 years)[30], the torso mass percentage (from T1 to L5) in current study followed the same trend, Figure 8. Data for Duval-Beaupère from T1 to T3 were omitted because of the addition arm mass for valid comparison. The overall torso mass percentage was 34.28%, higher than 30.70% reported by Pearsall et al and 27.8% reported by Keenan et al.

The LR-centroid and AP-centroid coordinates were referenced to that of T3. The average LR-centroid and AP-centroid were 3.40(SD 8.94) mm and -13.88(SD 8.67) mm respectively, similar to that calculated by Keenan et al. [13], LR-centroid of 3.34(SD 2.37) mm and AP-centroid of -21.52(SD 9.93) mm. Due to the tissue in the cervical level was closer to the A-side compared to that in T3, centroids from the cervical level deviated most, with LR-centroid of 5.18(SD 12.93) mm and AP-centroid of -21.24(SD 16.22) mm.

Table 4: Torso soft tissue parameter – Algorithm 4. The LR-centroid and AP-centroid coordinates were referenced to that of T3.

Level	Area (SD) mm ²	Volume (SD) cm ³	Mass (SD) g	Mass Percentage (SD) %	LR-Centroid (SD) mm	AP-Centroid (SD) mm
C1	24396.87(0.00)	357.78(0.00)	372.09(0.00)	0.36(0.00)	-8.15(0.00)	-22.44(0.00)
C2	20773.87(4810.80)	390.89(76.26)	406.52(79.31)	0.51(0.24)	8.76(17.67)	-40.07(16.98)
C3	17202.36(5307.13)	330.74(117.91)	343.97(122.63)	0.40(0.03)	8.27(12.96)	-42.01(22.88)
C4	19829.25(14036.57)	368.21(261.04)	382.94(271.48)	0.42(0.20)	26.87(16.17)	-23.65(25.55)
C5	26365.25(22720.16)	431.39(358.96)	448.65(373.31)	0.49(0.30)	13.1(1.06)	-16.77(29.80)
C6	35170.04(19574.33)	559.91(312.01)	582.31(324.49)	0.66(0.20)	-8.02(19.89)	-4.57(13.78)
C7	45027.69(13787.74)	782.1(349.44)	813.38(363.41)	0.93(0.16)	-4.57(12.25)	0.86(6.10)
T1	52377.65(10132.77)	1145.8(218.22)	1191.63(226.94)	1.42(0.13)	-3.16(8.57)	0.77(4.83)
T2	54128.11(9104.38)	1259.67(201.22)	1310.06(209.27)	1.57(0.20)	-0.29(1.45)	0.13(2.90)
T3	63645.93(17237.47)	1428.66(291.30)	1485.81(302.95)	1.65(0.02)	0(0.00)	0(0.00)
T4	62229.41(14139.21)	891.42(746.22)	927.08(776.07)	1.70(0.17)	-8.9(16.41)	-1.29(1.29)
T5	60141.18(15171.34)	905.48(738.30)	941.69(767.83)	1.69(0.16)	-16.56(12.93)	-2.53(4.47)
T6	55603.92(15256.78)	512(793.06)	532.48(824.78)	1.52(0.12)	9.94(11.68)	-5.85(4.66)
T7	55188.44(19218.86)	758.73(644.43)	789.08(670.21)	1.49(0.26)	3.79(3.37)	-10.54(4.04)
T8	61538.63(23448.44)	619.96(974.47)	644.76(1013.45)	1.75(0.41)	1.99(3.75)	-15.01(5.90)
T9	63950.16(24493.05)	697.45(1107.19)	725.35(1151.48)	1.87(0.43)	4.17(3.21)	-17.22(4.49)
T10	64752.19(23357.97)	759.54(1211.97)	789.92(1260.44)	2.06(0.37)	2.97(4.70)	-18.17(5.19)
T11	68779.24(21125.38)	1551.23(1306.46)	1613.28(1358.72)	2.25(0.22)	5.44(8.78)	-20.81(3.62)
T12	66650.32(19605.67)	1571.26(1323.54)	1634.11(1376.48)	2.30(0.19)	4.17(9.89)	-20.26(2.53)

L1	67532.15(19564.73)	2350.66(2070.75)	2444.69(2153.58)	2.67(0.40)	5.17(13.30)	-21.71(2.99)
L2	65877.53(20251.69)	1830.74(1558.77)	1903.97(1621.13)	2.64(0.32)	6.49(15.77)	-17.44(3.60)
L3	66715.49(24501.78)	1796.73(1522.78)	1868.6(1583.69)	2.46(0.51)	8.95(12.19)	-14.58(7.35)
L4	65539.61(26307.60)	2220.09(870.31)	2308.89(905.12)	2.49(0.55)	10.48(13.29)	-10.03(10.85)
L5	65482.39(24568.75)	2475.74(1098.67)	2574.77(1142.61)	2.75(0.78)	10.67(16.24)	-9.98(8.40)

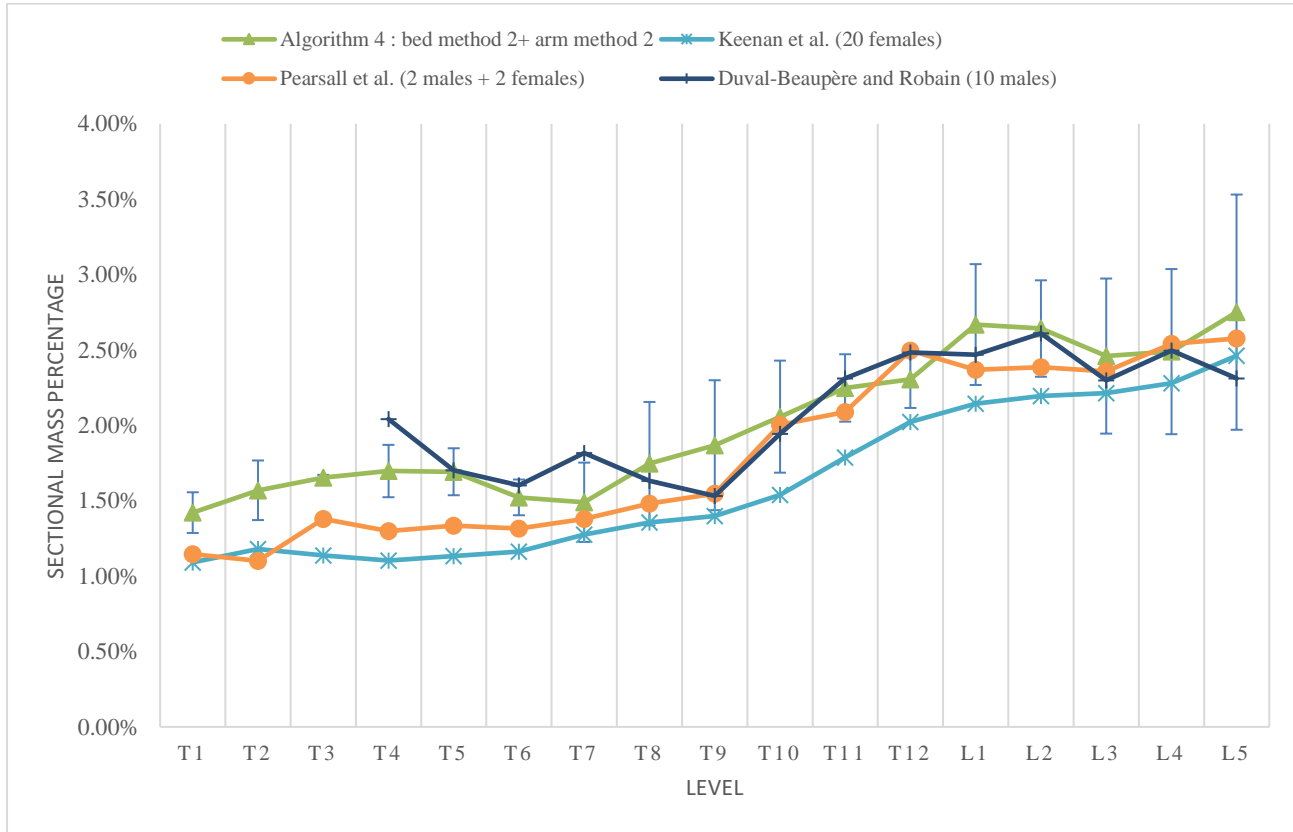


Figure 8: Average torso mass percentage (from T1 to L5) by Algorithm 4 in the current study and from the studies by Keenan et al. Pearsall et al. and Duval-Beaupère and Robain, where the error bars represented the standard deviation for this study.

Figure 9 shows the average AP results for each section of the 3 databases for area evaluation. The APs of all vertebral levels from C1 to L5 by the 4 combined algorithms were all above 95%, and the average was 98.84(SD 1.06)%. These 4 algorithms showed the least segmenting accuracy in level T7, with an average AP of 97.11(SD 0.92)%, while the best accuracy in C5, with an average AP of 99.94(SD 0.02)%. The 4 combined algorithms performed the best in cervical sections, with an average AP of 99.65 (SD 0.57)%, while performed the worst in lumbar sections, with an average AP of 98.04 (SD 0.60)%. The average APs of Algorithm 1, 2, 3 and 4 were 98.65(SD 1.36)%, 98.60(SD 1.34)%, 99.28(SD 0.55)%, 99.24(SD 0.58)% respectively. Compared Algorithm 1 and 2 (both used arm removal method 1) with Algorithm 3 and 4 (both used arm removal method 2), arm removal method 2 (watershed algorithm) showed an advantage at segmenting torso soft tissue. However, there was little difference in AP between CT bed scanner removal method 1 and method 2 when comparing Algorithm 1 and 3 (both used CT scanner bed method 1) with Algorithm 2 and 4 (both used CT scanner bed method 2).

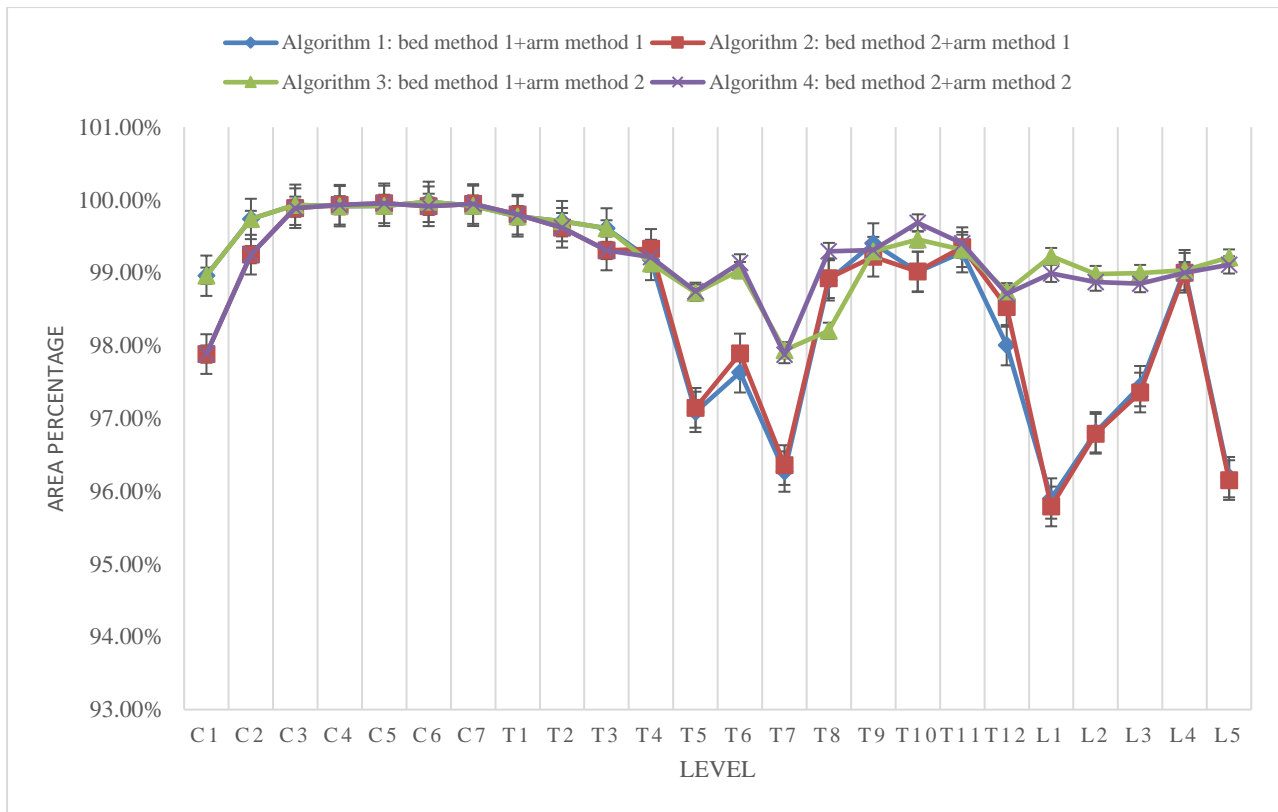


Figure 9: Average area percentage of the torso soft tissue segmentation results.

4. Discussion

The torso soft tissue segmentation algorithm developed in this study provided routes to speed up the spine modelling process. Key parameters, including area, volume, mass, and mass percentage were calculated to evaluate the efficiency of this algorithm. Automated soft tissue segmentation could be easily realised using some commercial software like MIMICS or ImageJ[13], but none of them includes automated CT bed removal and arm removal, which need to be done manually. This study automated the entire process successfully and can now be readily used.

4.1. Algorithm optimisation

CT scanner bed removal method 2 optimisation

Method 2 was 4 times on average faster than method 1, but less automated. It required selecting one transverse slice that torso and CT bed need to be separated and bed projection needs to be obvious, in case the torso and bed could not be separated in other slices resulting in Figure 10. Therefore, the cervical slice searching algorithm can be developed to find the slices where the CT bed and torso are separated. In addition, the CT bed projection may be enhanced by summing up the bed projection of multiple slices.

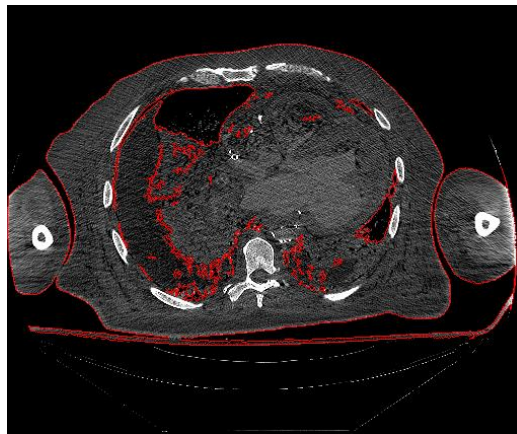
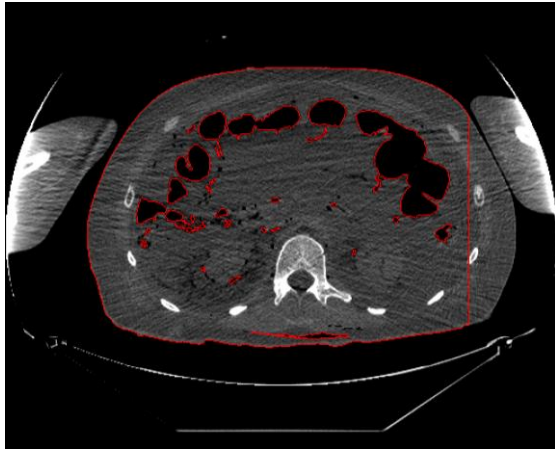


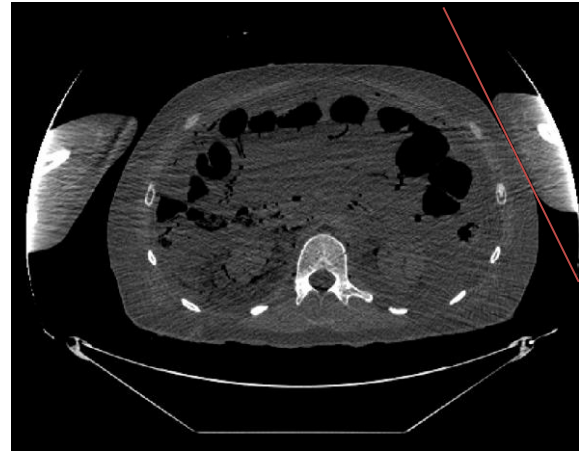
Figure 10: Soft tissue region when torso and CT bed are not separated by CT scanner bed method 2.

Arm removal method 1 optimisation

Method 1 showed a high accuracy of torso soft tissue segmentation with both DC and AP above 97% on average. However, it didn't work well if the specimen put the forearms on the abdomen (specimen 636 and 526), Figure 11(a), as the algorithm could only detect the peak along the LR axis, thus only worked for cutting left and right arms. Therefore, an algorithm for detecting the peaks in multiple directions may be considered. The arms could be cut through the line, Figure 11(b), after selecting the peaks with the highest prominence. In addition, the parameters for peak detection were typically set manually to the required peak height of 50, the required minimum horizontal distance between the two peaks of 200 pixels, the peak width and prominence of 1. These settings could differ from different slices, which may need an algorithm to improve that.



(a)

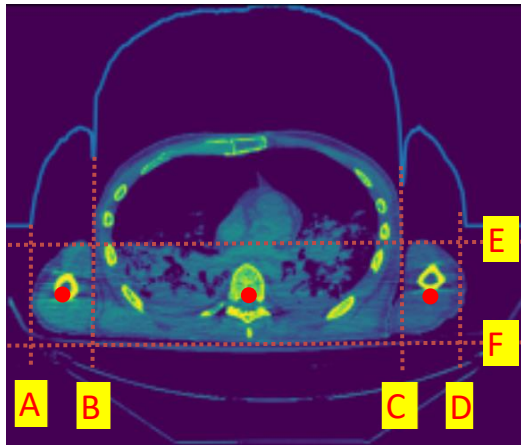


(b)

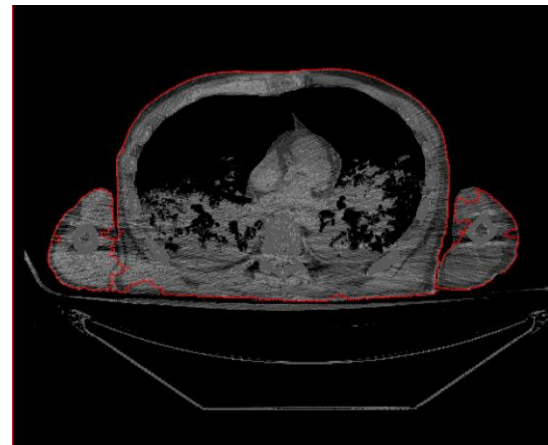
Figure 11: (a) Torso soft tissue segmentation result (red contours) of specimen 526 using arm removal method 1. (b) Not cutting arms in AP axis (red line).

Arm removal method 2 optimisation

Method 2, the watershed algorithm, was good at detecting the edges between arms and torso but could easily cause over-segmentation due to the grayscale value ununiform in the soft tissue region even after removing the bone contrast. This may be improved by combining filters for image denoising and edge enhancement[31]. Moreover, as this algorithm required manually marker settings and was sensitive to those, an automated marker setting algorithm could be developed. One attempt was to set the markers' centroids whose LR-coordinates to be the midpoint of AB, BC and CD, and AP-coordinates to be the midpoint of EF, Figure 12 (a), resulting in the segmentation results shown in Figure 12(b). This process used peak detection in Method 1, therefore it is only suitable for the arms located on the left and right sides of the torso, which could be optimised by the peak detection optimisation mentioned above.



(a)



(b)

Figure 12: (a) Automated markers' centroids in red points, where points E and F represent the upper and lower ends of the arms. (b) Arm and torso segmentation results (in red contours) using automated marker setting.

4.2. GUI framework

To improve the user-friendliness of this algorithm, a graphic user interface (GUI) is worthy of developing, with the proposed flowchart shown in Figure 13. Considering the differentials of those methods, method 2 in 2.3 would be the first choice for CT scanner bed removal as its fast speed, while method 1 could be considered when there is no suitable slice for detecting the bed projection. Method 1 in 2.5 would be the first choice to remove the arms, then method 2 could be applied for those slices which are not well segmented. Based on the segmentation result, the masses and centroids could be calculated used in spine modelling. The python GUI framework PyQt is recommended as it could run on all platforms.

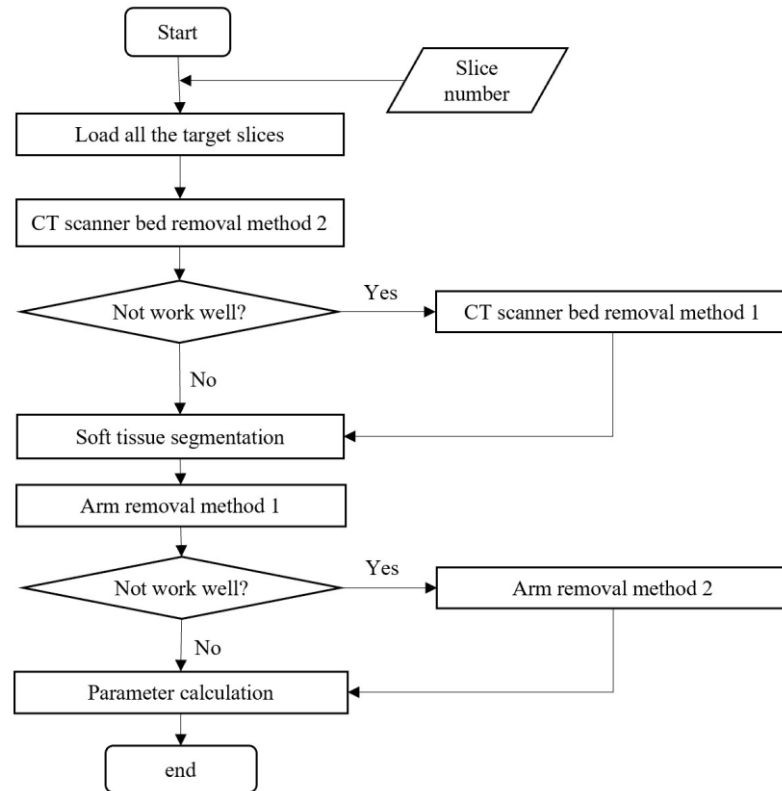


Figure 13: Graphic user interface proposed flowchart.

5. Conclusion

An automated torso soft tissue segmentation algorithm for calculating the masses and centroids was developed to address the time-consuming and user-fatigue problem caused by manual segmentation in spine modelling. This algorithm consisted of 3 parts: CT scanner bed removal, soft tissue segmentation and arm removal, where 2 various methods were developed for each of CT bed removal and arm removal. The combination of CT scanner bed removal method 2 and arm removal method 2 gave the best outcome as measure by the DC of 98.32%, and the computation time of 8.79 s per slice. In addition, the parameters (masses and centroids) for spine modelling were calculated, with the overall torso mass percentage of 34.82%. This program can be readily used and are worthy of improving by algorithm optimisation and GUI.

6. References

- [1] K. Gupta and A. J. Przekwas, "A Framework for Multiscale Modeling of Warfighter Blast Injury Protection."
- [2] J. C. Roberts, E. E. Ward, T. P. Harrigan, T. M. Taylor, M. A. Annett, and A. C. Merkle, "Development of a Human Head-Neck Computational Model for Assessing Blast Injury." [Online]. Available: http://asmedigitalcollection.asme.org/IMECE/proceedings-pdf/IMECE2009/43758/95/2750013/95_1.pdf
- [3] A. M. Pearson *et al.*, "Frontal impact causes ligamentous cervical spine injury," *Spine*, vol. 30, no. 16, pp. 1852–1858, Aug. 2005, doi: 10.1097/01.BRS.0000174117.42046.63.
- [4] G. S. Gluck, J. A. Bendo, and J. M. Spivak, "The lumbar spine and low back pain in golf: a literature review of swing biomechanics and injury prevention," *The Spine Journal*, vol. 8, no. 5, pp. 778–788, Sep. 2008, doi: 10.1016/J.SPINEE.2007.07.388.
- [5] A. Jalalian, I. Gibson, and E. H. Tay, "Computational biomechanical modeling of scoliotic spine: Challenges and opportunities," *Spine Deformity*, vol. 1, no. 6, pp. 401–411, Nov. 2013, doi: 10.1016/j.jspd.2013.07.009.
- [6] T. P. C. Schlösser *et al.*, "Anterior Overgrowth in Primary Curves, Compensatory Curves and Junctional Segments in Adolescent Idiopathic Scoliosis," *PLOS ONE*, vol. 11, no. 7, p. e0160267, Jul. 2016, doi: 10.1371/JOURNAL.PONE.0160267.
- [7] C. Coillard, V. Vachon, A. Circo, M. Beauséjour, N. Shawafaty, and C. H. Rivard, "Effectiveness of the Spinecor brace based on the new standardized criteria proposed by the Scoliosis Research Society for adolescent idiopathic scoliosis," vol. 88, no. 2, p. 21, 2002, doi: 10.1186/1748-7161-2-S1-S21.
- [8] J. P. Little and C. Adam, "Towards determining soft tissue properties for modelling spine surgery: current progress and challenges", doi: 10.1007/s11517-011-0848-6.
- [9] X. Ye *et al.*, "Lumbar Spine Response of Computational Finite Element Models in Multidirectional Spaceflight Landing Conditions," *Journal of Biomechanical Engineering*, vol. 142, no. 5, May 2020, doi: 10.1115/1.4045401.
- [10] Z. L. Wang *et al.*, "Computational biomechanical modelling of the lumbar spine using marching-cubes surface smoothened finite element voxel meshing," *Computer Methods and Programs in Biomedicine*, vol. 80, no. 1, pp. 25–35, Oct. 2005, doi: 10.1016/j.cmpb.2005.06.006.
- [11] D. W. van Lopik and M. Acar, "Development of a multi-body computational model of human head and neck," *Proceedings of the Institution of Mechanical Engineers, Part K: Journal of Multi-body Dynamics*, vol. 221, no. 2, pp. 175–197, 2007, doi: 10.1243/14644193JMBD84.
- [12] Z. Gao, I. Gibson, C. Ding, J. Wang, and J. Wang, "Virtual Lumbar Spine of Multi-body Model Based on Simbody," *Procedia Technology*, vol. 20, pp. 26–31, 2015, doi: 10.1016/j.protcy.2015.07.006.
- [13] B. E. Keenan *et al.*, "Segmental torso masses in adolescent idiopathic scoliosis," *Clinical Biomechanics*, vol. 29, no. 7, pp. 773–779, Aug. 2014, doi: 10.1016/j.clinbiomech.2014.06.002.
- [14] B. Foldyna *et al.*, "CT evaluation prior to transapical aortic valve replacement: semi-automatic versus manual image segmentation," *The International Journal of Cardiovascular Imaging*, doi: 10.1007/s10554-015-0662-6.
- [15] K. Popuri, D. Cobzas, N. Esfandiari, V. Baracos, and M. Jägersand, "Body composition assessment in axial CT images using FEM-based automatic segmentation of skeletal muscle," *IEEE Transactions on Medical Imaging*, vol. 35, no. 2, pp. 512–520, Feb. 2016, doi: 10.1109/TMI.2015.2479252.
- [16] J. C. M. Than, N. M. Noor, O. M. Rijal, A. Yunus, and R. M. Kassim, "Lung segmentation for HRCT thorax images using radon transform and accumulating pixel width," *IEEE TENSYP 2014 - 2014 IEEE Region 10 Symposium*, pp. 157–161, Jul. 2014, doi: 10.1109/TENCONSPRING.2014.6863016.
- [17] E. E. Nithila and S. S. Kumar, "Segmentation of lung nodule in CT data using active contour model and Fuzzy C-mean clustering," *Alexandria Engineering Journal*, vol. 55, no. 3, pp. 2583–2588, Sep. 2016, doi: 10.1016/J.AEJ.2016.06.002.
- [18] S. Dai, K. Lu, J. Dong, Y. Zhang, and Y. Chen, "A novel approach of lung segmentation on chest CT images using graph cuts," *Neurocomputing*, vol. 168, pp. 799–807, Nov. 2015, doi: 10.1016/J.NEUCOM.2015.05.044.
- [19] P. K. Sahoo, S. Soltani, and A. K. C. Wong, "A survey of thresholding techniques," *Computer Vision, Graphics, and Image Processing*, vol. 41, no. 2, pp. 233–260, Feb. 1988, doi: 10.1016/0734-189X(88)90022-9.

- [20] K. Sreedhar and B. Panlal, "Enhancement of Images using Morphological Transformation," *International Journal of Computer Science and Information Technology*, vol. 4, no. 1, pp. 33–50, Mar. 2012, doi: 10.5121/ijcsit.2012.4103.
- [21] R. R. Shamir, Y. Duchin, J. Kim, G. Sapiro, and N. Harel, "Continuous Dice Coefficient: a Method for Evaluating Probabilistic Segmentations," Jun. 2019, Accessed: Sep. 06, 2021. [Online]. Available: <https://arxiv.org/abs/1906.11031v1>
- [22] F. Milletari, N. Navab, and S. A. Ahmadi, "V-Net: Fully convolutional neural networks for volumetric medical image segmentation," *Proceedings - 2016 4th International Conference on 3D Vision, 3DV 2016*, pp. 565–571, Dec. 2016, doi: 10.1109/3DV.2016.79.
- [23] A. M. Bailey, J. J. Christopher, R. S. Salzar, and F. Brozoski, "Comparison of Hybrid-III and Postmortem Human Surrogate Response to Simulated Underbody Blast Loading," *Journal of Biomechanical Engineering*, vol. 137, no. 5, May 2015, doi: 10.1115/1.4029981.
- [24] A. A. Abd Rahni, M. F. Mohamed Fuzaie, and O. I. al Irr, "Automated bed detection and removal from abdominal CT images for automatic segmentation applications," *2018 IEEE EMBS Conference on Biomedical Engineering and Sciences, IECBES 2018 - Proceedings*, pp. 677–679, Jan. 2019, doi: 10.1109/IECBES.2018.8626638.
- [25] L. Chen, S. Wu, Z. Zhang, S. Yu, Y. Xie, and H. Zhang, "Real-Time Patient Table Removal in CT Images," *Lecture Notes in Computer Science (including subseries Lecture Notes in Artificial Intelligence and Lecture Notes in Bioinformatics)*, vol. 10038 LNCS, pp. 1–8, 2016, doi: 10.1007/978-3-319-48335-1_1.
- [26] Y.-M. Zhu, S. M. Cochoff, and R. Sukalac, "Automatic Patient Table Removal in CT Images", doi: 10.1007/s10278-012-9454-x.
- [27] L. Gong, S. Pathak, A. Alessio, and P. Kinahan, "Automatic arm removal in PET and CT images for deformable registration," *Computerized Medical Imaging and Graphics*, vol. 30, no. 8, pp. 469–477, Dec. 2006, doi: 10.1016/j.compmedimag.2006.09.013.
- [28] H. P. Ng, S. H. Ong, K. W. C. Foong, P. S. Goh, and W. L. Nowinski, "Medical image segmentation using k-means clustering and improved watershed algorithm," *Proceedings of the IEEE Southwest Symposium on Image Analysis and Interpretation*, vol. 2006, pp. 61–65, 2006, doi: 10.1109/SSIAI.2006.1633722.
- [29] D. J. Pearsall, J. G. Reid, and L. A. Livingston, "Segmental inertial parameters of the human trunk as determined from computed tomography," *Annals of Biomedical Engineering* 1995 24:2, vol. 24, no. 2, pp. 198–210, 1996, doi: 10.1007/BF02667349.
- [30] G. Duval-Beaupère and G. Robain, "Visualization on full spine radiographs of the anatomical connections of the centres of the segmental body mass supported by each vertebra and measured in vivo," *International Orthopaedics* 1987 11:3, vol. 11, no. 3, pp. 261–269, Aug. 1987, doi: 10.1007/BF00271459.
- [31] U. Mittal and S. Anand, "Modified Watershed Segmentation with Denoising of Medical Images," *International Journal of Innovative Research in Science, Engineering and Technology*, vol. 2, 2013, [Online]. Available: www.ijirset.com

7. Annexes

7.1. Slice height results and vertebral body centroids using Method 4

Table 5: Slice height results and vertebral body centroids for specimen 606

Level	VBH mm	IDH (Level to Level+1) mm	c_z
C2	20.74	4.86	215.71
C3	14.65	3.75	237.96
C4	14.41	4.13	257.10
C5	14.40	2.84	276.89
C6	13.31	2.59	294.64
C7	15.17	5.10	311.62
T1	18.21	3.72	329.80
T2	20.22	3.21	349.73
T3	19.49	3.58	369.21
T4	18.81	4.16	390.44
T5	21.73	4.37	411.60
T6	20.18	3.54	437.38
T7	19.30	4.16	461.15
T8	19.91	4.11	485.68
T9	21.05	3.77	511.14
T10	22.32	5.25	536.80
T11	22.96	5.88	565.51
T12	24.63	5.79	595.81
L1	25.68	6.52	626.58
L2	28.42	7.10	660.39
L3	27.62	3.68	696.00
L4	28.13	6.16	728.38
L5	30.61	2.02	765.29

Table 6: Slice height results and vertebral body centroids for specimen 636

Level	VBH mm	IDH (Level to Level+1) mm	c_z
T3	18.11	3.20	298.99
T4	20.76	3.88	320.455
T5	19.74	3.31	344.452
T6	18.75	3.87	367.205
T7	18.75	4.30	390.403
T8	20.36	4.71	414.427
T9	20.71	4.74	439.962
T10	20.89	5.83	466.03
T11	21.76	6.04	493.501
T12	22.95	6.55	522.126
L1	24.60	7.79	552.831
L2	24.23	5.63	585.244
L3	25.52	6.29	616.484

L4	26.71	7.48	649.125
L5	25.84	11.15	683.388

Table 7: Slice height results and vertebral body centroids for specimen 526

Level	VBH mm	IDH (Level to Level+1) mm	c_z
C1	11.58	3.08	171.996
C2	11.24	2.70	185.519
C3	15.69	4.07	208.871
C4	14.56	4.02	228.934
C5	13.18	2.97	247.062
C6	12.72	3.21	262.915
C7	14.72	4.07	278.963
T1	18.30	3.53	296.955
T2	19.12	4.02	316.333
T3	21.98	3.90	334.398
T4	19.85	3.28	359.965
T5	20.50	3.70	384.01
T6	21.10	4.28	409.379
T7	20.39	4.34	435.482
T8	21.29	4.88	460.98
T9	22.76	4.65	488.317
T10	23.78	6.45	517.005
T11	23.64	6.80	547.925
T12	26.11	6.04	580.025
L1	28.02	11.20	612.674
L2	27.75	10.84	652.318
L3	29.06	6.24	692.046
L4	30.57	4.54	728.948
L5	34.20	6.18	767.081

7.2. Length of the sagittal and coronal images

Table 8: Length of the sagittal and coronal images

Specimen	Length
606	1024
636	961
526	863